Acrylic-Based Nanocomposite Resins for Coating Applications

M. L. Nobel, E. Mendes, S. J. Picken

Polymer Materials and Engineering, Faculty of Applied Sciences, Delft University of Technology, 2628 BL Delft, The Netherlands

Received 25 November 2005; accepted 23 February 2006
DOI 10.1002/app.24318
Published online in Wiley InterScience (www.interscience.wiley.com).

ABSTRACT: Acrylic-based nanocomposite resins have been investigated in view of future application in water borne automotive coatings by the aid of postemulsification processes. Mechanical, flow and leveling properties of the nanocomposite resins, containing various concentrations of silicate, have been investigated. The results are related to morphological information obtained from TEM and WAXS measurements in the liquid suspension as well as from the cured film. At low silicate loadings, when flow properties are still acceptable for typical emulsification processing, a strong increase in modulus of the cured coating films is observed because of the mainly exfoliated silicate platelets. The rate of increase in modulus of the cured films decreases at higher silicate loadings. Analyzing the mechanical data, using Halpin–Tsai theory indicates that this is due to less perfect exfoliation at higher silicate loading, which is confirmed by TEM analysis. In addition at higher silicate loading, the flow properties of the resin as analyzed by DMA show solid-like behavior. This can lead to poor film formation in future application. © 2007 Wiley Periodicals, Inc. J Appl Polym Sci 104: 2146–2156, 2007

Key words: acrylic resin; nanocomposite; organic layered silicate

INTRODUCTION

Mineral fillers, metals, and fibers have been added to thermoplastics and thermosets for many years to form composites.[1] Compared with the unfilled polymer system, these composites have a number of improved properties including tensile strength, heat distortion temperature, and modulus. More recently, advances in synthetic techniques and the ability to readily characterize materials on an atomic scale has led to interest in nanometer-size particles. Polymer nanocomposites combine the two concepts of composites and nanometer-size particles. But the properties of a (nano)composite are not simply the sum of the properties of the components. The composite properties are also determined by the size, shape, and spatial distribution of the filler particles in the matrix and by the forces acting between the components.[1] It has been found that decreasing the average size of the fillers from a few micrometers to a few nanometers can result in a higher gain in yield stress and modulus. The most important parameter for the altered behavior of nanocomposite particles compared with that of conventional filled materials is the dramatically increased surface area of the filler. This surface area is a factor, since interactions between the filler and the matrix are very important for the final composite properties. Some of the properties of nanocomposites, such as increased tensile strength, are achieved using much lower filler loading, thereby gaining in terms of reduced weight and increased transparency and gloss. Other properties of nanocomposites, such as clarity or improved barrier properties cannot be duplicated by conventionally-filled resins at any loading level.

Nanostructured composites of montmorillonite type silicates embedded within various polymer matrices have been intensively studied in recent years. Technological interest in these types of layered nanocomposites is spurred by their enhanced mechanical and barrier properties, compared with that of conventional composites. Most of these materials are, however, processed or commercialized in organic solvents, and environmental regulations in automotive production procedures places the use of solvent based (SB) lacquer systems under increased pressure. As a consequence, there is a growing need for less environmental unfriendly alternatives such as solvent free lacquer systems raising the interest, for instance, on water borne (WB) systems. These contain substantially less solvent and are easy to produce. A disadvantage is that up to now they contain components that are far more expensive than the components of SB systems. Moreover, it is harder (and therefore more expensive) to obtain the same product quality as SB lacquer systems. The practical application of our research is

Correspondence to: M.L. Nobel (marie.louise.nobel@corusgroup.com).

Contract grant sponsors: Ministry of Economic Affairs, Education, Culture, and Sciences; Ministry of Housing, Spatial Planning, and the Environment; Senter and Novem.

Journal of Applied Polymer Science, Vol. 104, 2146–2156 (2007)

aimed to develop an innovative technology for WB nanocomposite resin systems, yielding automotive coatings with a superior mix of material and application properties.[2] The desired improvements include scratch resistance, chemical degradation resistance, and improved mechanical properties, which may result from the synergistic effects of the organic and inorganic components. The effects of different nanoparticles on the properties of polymers vary a lot depending on the system, and so this requires more detailed analysis. In this article, motivated by the possibility of preparing WB systems via inverse emulsification, we focus on the analysis of a high performance organic SB automotive resin system, that is known to be emulsifiable in water.[3] In this article, the study of the structure and flow properties of the oligomers/nanoparticulate mixture in organic solvent is described, as well as the relation between the obtained cured films and their morphology and performance.

EXPERIMENTAL

Materials

The organic layered silicate (OLS) used for the preparation of the polyacrylate nanocomposite coatings was supplied by Southern Clay Products (Gonzales, TX) under the trade name Cloisite 30B. It is a natural montmorillonite treated with an organic modifier. Montmorillonite is a clay with a low content of aluminum, sodium, iron, and magnesium. It belongs to the smectite family and is found in the shape of thin sheets consisting of three layers. These layers consist of octahedral and tetrahedral planes in which certain atoms can be replaced by others. Thus, the silicon of tetrahedral layers can be replaced by aluminum, whereas in the octahedral layers, aluminum atoms can leave the network and can be replaced by various elements such as iron or magnesium. These substitution mechanisms give rise to a deficit of electronic charge that can be compensated by ions or other interfoliated layers.

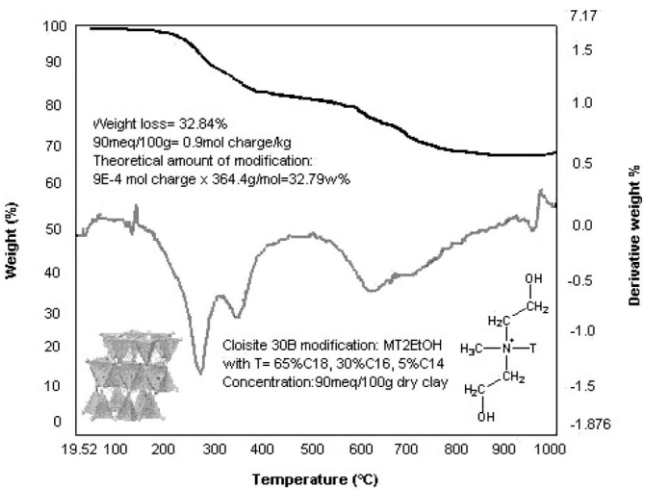

Figure 1 TGA curves of organoclay Cloisite 30B. The inset shows structural information of the organomodification.

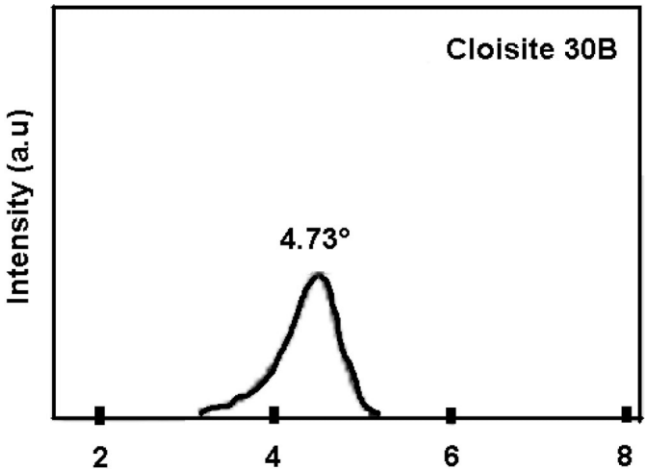

Figure 2 X-ray diffraction powder pattern of organoclay Cloisite30B. The basal spacing of C30B is shown to be 1.8 nm (4.73° 2è).

The ammonium cations present in Cloisite 30B (C30B) are methyl tallow bis-2-hydroxyethyl quaternary ammonium, at a modifier concentration of 90 meq/100 g. This value is related to the cationic exchange capacity of the clay, which in this case is utilized to 90 cmol of charge per kg clay. The basal spacing, d, of C30B is 1.8 nm, as measured by X-ray diffraction using Bragg's law, $n\lambda = 2d\sin\theta$, from the position of the (001) peak. Figures 1 and 2 give the structural information, weight loss upon heating, and the X-ray diffraction pattern of the organoclay. The material is available in the form of a fine powder. The clay was dried for 48 h at 80°C, hereby removing 2% of internal moisture before processing.

A resin formulation was selected as a model system to study the influence of OLS. BASF patent US 5670,600 relates to the invention of a two component aqueous polyurethane coating composition comprising a water dilutable polyacrylate resin and a polyisocyanate component as a crosslinking agent. The aqueous polyacrylate resin is obtainable via a two-step solution polymerization. On the basis of the examples stated in this patent, Nuplex Resins synthesized an oligomer solution in ethoxyethyl propionate. After composite preparation, these can be emulsified in a next stage via addition of water and removal of the organic solvent. Table I provides the composition and characteristics of the synthesized solvent-based polyacrylate resin used for composite preparation.

As a crosslinking agent for this system, Nuplex Resins provides US138BB-70, a solution of nonplasticized melamine resin with a very high reactivity, under the brand name Setamine.

TABLE I
Resin Formulation Composition and Characteristics

		Explanation
Composition		
Method	2 stage	
SV	30	Solvent mixture of butyl acetate and ethoxyethylpropionate
Cardura E10	10	Glycidyl ester of versatic acid
n-BMA	20	*n*-butyl metacrylate
MMA	16	Methyl methacrylate
Styrene	15.4	
EHA	10	Ethylhexyl acetate
HEMA	22	Hydroxyethyl methacrylate
AA	6.6	Acrylic acid
TBPEH	6.0	t-Butyl perethylhexanoaat
Characteristics		
Nonvolatile (%)	73.2	Solids content in %
AN (mg KOH/g)	34.8	Acid number in mg KOH/g
Visc (Pa s)	ntb	Viscosity in Pa s at 23°C determined by Physica
Appearance	Clear	Color 68 APAH determined by SBM 008F

Composition (in parts) and characteristics of the solvent based polyacrylate resin prepared according to U.S. Pat. No. 5,670,600.

Compounding and preparation of polyacrylate nanocomposites

The synthetic route of choice for making a nanocomposite depends on whether the final material is required as an intercalated or exfoliated system. In the case of an intercalate, the organic component is inserted between the layers of the clay such that the interlayer spacing is expanded, but the layers still have a well-defined spacing. In an exfoliated structure, the layers of the clay are completely separated and the individual silicate sheets are distributed throughout the organic matrix. A third alternative is dispersion of the clay powder particles (tactoids) within the polymer matrix, but this simply represents use of the clay as a conventional filler. The correct selection of modified clay is essential to ensure effective penetration of the polymer or its precursor into the interlayer spacing of the clay so as to obtain the desired exfoliated or intercalated product. Polymers can be incorporated either as the polymer itself or via the monomer, which is polymerized *in situ* to give the corresponding polymer–clay nanocomposite. Polymers can be introduced by melt blending, for example extrusion, or by solution blending. Melt blending (compounding) depends on shear, to help delaminate the clay and can be less effective than *in situ* polymerization to produce an exfoliated nanocomposite.

The polyacrylate nanocomposites are prepared as shown in Scheme 1.

C30B powder is swollen in xylene under high shear (6000 rpm). After 20 min, 1,2-propylene carbonate (PC) is added still under high shear (C30B/PC = 1:1). This polar activator weakens the van der Waals forces that are keeping the platelets together. As a consequence, within 15 min, a large viscosity increase is observed because of the increased spacing between the platelets and the occurrence of OH—bridging via the platelet edges. To promote exfoliation at this stage, 15 min of simultaneous ultrasonication is applied. Dispersion by ultrasound is a consequence of microturbulence caused by fluctuations of pressure and by cavitation. Cavitation bubbles expand and subsequently implode within a very short time. The implosions locally result in very high pressures and temperatures.

To block the platelet edges from OH—bridging, 1,1,1,3,3,3-hexamethyldisilazane (HMDS) is added at a fixed proportion with the PC/clay addition: C30B/PC/HMDS = 1 : 1 : 1. As the mixture is still under high shear, the resin in solution is added and left under high shear for 30 min. The obtained composite resins consisting of a oligomer/nanoparticle mixture in organic solvent are used for rheological and X-ray diffraction analysis. After completing this resin composite preparation, the crosslinker is added in a ratio of resin/crosslinker = 70 : 30. Films are cast on a polypropylene substrate with a doctor blade gap of 200 μm. After curing for 1.5 h at 140°C, free coating films of ~150 μm can be obtained. The performance and structure of the obtained free nanocomposite coating films are analyzed by means of DMTA, X-ray diffraction, and TEM. For further research, an emulsion in water can also be prepared, as shown in Scheme 1.

Analysis techniques

Transmission electron microscopy

Transmission electron microscopy (TEM) was performed using a Philips CM30T electron microscope

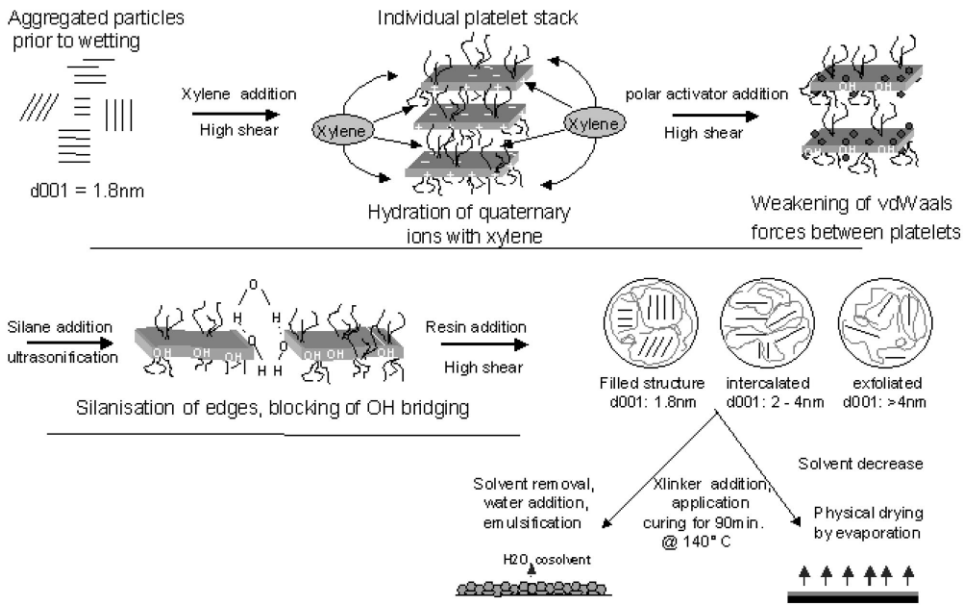

Scheme 1 Scheme of nanocomposite preparation.

with a LaB6 filament operated at 300 kV. Samples were mounted on Quantifoil ® carbon polymer supported on a copper grid, by placing some ultramicrotomed-slices on the grid. Four cured acrylic films, with varying clay content in the range of 0.5–8 wt %, were studied using this technique.

Dynamic mechanical thermal analysis

Dynamic mechanical measurements (DMTA) were carried out using a modified Rheovibron (Toyo Baldwin, type DDV-II-C) at a frequency of 11 Hz with a dynamic strain of 0.03%. The temperature was varied between −50 and 200°C at a heating rate of 5°C/min.

To keep the sample sufficiently loaded during the experiment (to keep the sample flat), a static force F_{sta} is applied on the sample. As the stiffness of the sample changes with temperature, the static force level is adjusted at each temperature. In the glassy state and in the glass transition temperature region, the static stress is set at five times the dynamic stress as results from the applied dynamic strain of 0.03%.

In the rubber region, a constant static stress is applied on the sample. This static stress is typically 0.4 MPa.

The samples were stamped from a free standing film of the coating, using a special cutting device placed in a press. The width and length of the clamped samples was 3 and 30 mm, respectively.

The thickness of the sample was determined using an inductive thickness gauge (Isoscope® MP, Fischer Instrumentation). The thickness was determined on at least five different spots on the sample and the average thickness and the standard deviation were determined.

All measurements were done in tensile mode and at each temperature the tensile storage modulus E', the tensile loss modulus E'', and the value of the tan δ (tan $\delta = E''/E'$) were determined.[4]

Thermogravimetric analysis

The exact amount of C30B in composite samples was determined by using TGA. The samples were heated from 25 to 1000°C at a rate of 50°C/min and were kept at this temperature for 30 min. Since the acrylic resin and the organic modification of C30B degraded completely without leaving any residue, the remaining part gave us the w/w concentrate of our filler. The amount of weight loss as observed by TGA on the pure Cloisite (in the form of dried powder) was taken into account in this measurement.

We note that the relationship between the weight fraction of the organic montmorillonite (OMM) and volume percentage of OMM platelets was calculated with eq. (1):

$$V_{\mathrm{OMM}} = \frac{w_{\mathrm{OMM}}\,\rho_{\mathrm{OMM}}{}^{1}}{w_{\mathrm{OMM}}\,\rho_{\mathrm{OMM}}{}^{1} + (1 - w_{\mathrm{OMM}})\rho_S{}^{-1}}$$

$$\text{with } \rho_{\mathrm{OMM}} = 1.98 \text{ g/cm and } \rho_{s=\mathrm{O-xylene}} = 0.88 \text{ g/cm} \quad (1)$$

The amount of surfactant on the MMT platelets was determined using TGA, which show a residue of 67.21

wt %, (weight loss by degradation of the crystal itself was taken into account.)

For example, compounding 5 wt %, C30B in the final cured film contains 0.024 volume fraction of MMT platelets (ρ_{OMM} = 1.98 g/cc and $\rho_{solvent,\ xylene}$ = 0.88 g/cc).

DMA-rheology

The rheological experiments were conducted on a controlled strain Rheometrics Ares rheometer equipped with a Couette geometry. The diameter of the bob and cup were 31.97 and 33.9 mm, respectively. The length of the bob was 33.35 mm. Steady shear rate and transient and oscillatory measurements were carried out to study the rheological behavior, with varying concentrations of filled acrylic polymer solutions. Between successive series of measurements, the solution was allowed to rest 30 min. All measurements were performed at room temperature.

X-ray diffraction

A Bruker-Nonius D8-Discover set-up with a 2D detector was used to perform the experiments. The sample to detector distance was set to 10 cm; the incident beam wavelength was 1.54 Å. Special attention was paid to sample preparation, and fluid resins were measured in a capillary to ensure a constant thickness and random orientation. Cured films were prepared in the absence of surface defects and at an overall thickness of 0.565 mm.

RESULTS AND DISCUSSION

Rheological properties of the resin composites by dynamic mechanical analysis

Preferably, coating systems for automotive purposes after application provide a good chemical and physical resistance as well as the smoothest possible surface with a certain amount of gloss. Before that result is accomplished, different phenomena occur at several stages of the paint application. Figure 3 gives an overview of the shear rates of the several processes.

A good rheological behavior of a paint system depends on several stages. During storage of the paint, the stability is affected by settling behavior. The brush- or spray-ablility of the paint influences the behavior during application. Finally, the ability to flow during film formation stage and the prevention of sagging during the curing stage will have a large influence on the performance of a paint system.

Unfortunately, water borne (WB) latex coatings do not possess the same rheological properties as solvent based (SB) coatings. If not correctly formulated, a latex paint can have inferior flow and leveling properties.

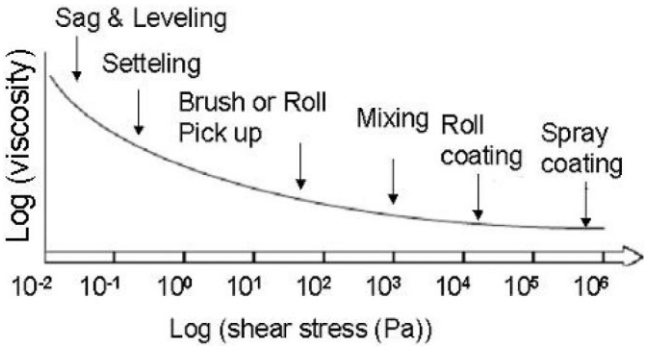

Figure 3 General viscosity versus shear stress profile occurring during various paint processing phenomena.

They may not give an adequate film formation, and can be plagued by spattering during application. The rheological properties of a complete coating formulation do not depend only on the resin that is used as the basis for the coating formulation. Always, fine-tuning is performed via the use of additives. At present, only the influence of the addition of nanoparticles on the bare resin is examined, i.e., the effect of additives is not considered.

The rheological experiments were conducted on a controlled strain Rheometrics Ares rheometer equipped with Couette geometry. Oscillatory measurements are performed to compare the rheological behavior of an acrylic-based resin containing an increasing amount of C30B to that of the pure acrylic resin at 55% solid content. Between successive measurements and after loading, the material was allowed to rest for 30 min under environmentally controlled conditions to prevent solvent evaporation. A series of dynamic strain sweeps were preformed to determine the linear region of deformation. At a temperature of 23°C and a deformation frequency of 1 rad/s, the viscoelasticity of the material becomes nonlinear at strains above 5%.

Frequency spectra were recorded in the linear region of deformation (5%strain). From this, the storage (G') and loss (G'') moduli as a function of volume percentage of clay were measured at different frequencies [Fig. 4(a,b)]. G' and G'' at an oscillation frequency of 5 rad/s, a typical frequency associated with the painting process, are shown in Figure 4(c) as a function of clay content.

The curves of the storage and loss moduli increase linearly with clay content. The features of the pure resin are the same as those found in a dilute solution of random coils. Incorporation of clay in the polymer matrix causes the curves to shift upwards. This behavior is also shown in Figure 5, which describes the viscosity of the filled resins as a function of shear stress.

The increase of the storage and loss moduli as shown in Figure 4(a,b) are characteristic for the addi-

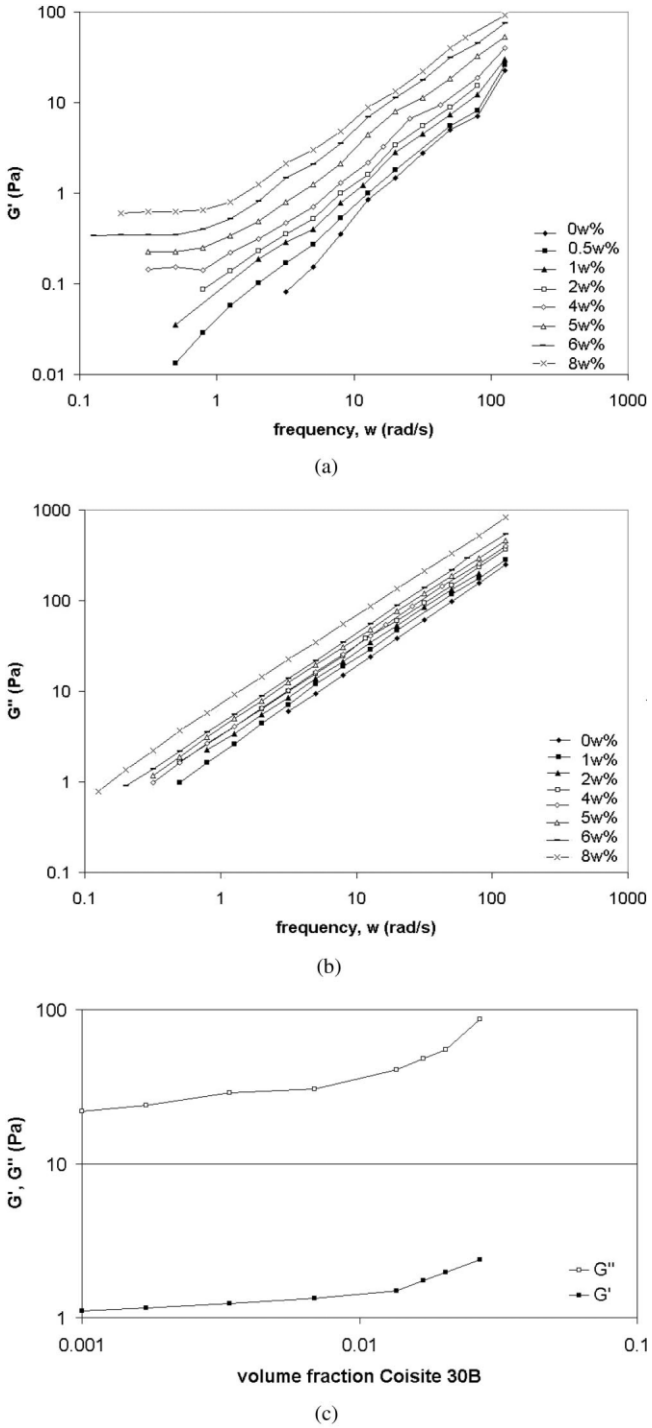

Figure 4 Storage and loss moduli of PNC resins containing increasing Cloisite 30B content. (a) Storage moduli at 5 Hz, (b) loss moduli at 5 Hz and (c) storage and loss moduli at 5 Hz as a function of volume fraction Cloisite 30B.

tion of a reinforcing-nanofiller to a polymer. From Figure 5, it can be seen that the resistance to flow increases at higher particle loadings. This build up of a yield stress is beneficial for sagging resistance, but it will have a negative effect on the coalescence during film formation from an emulsion.

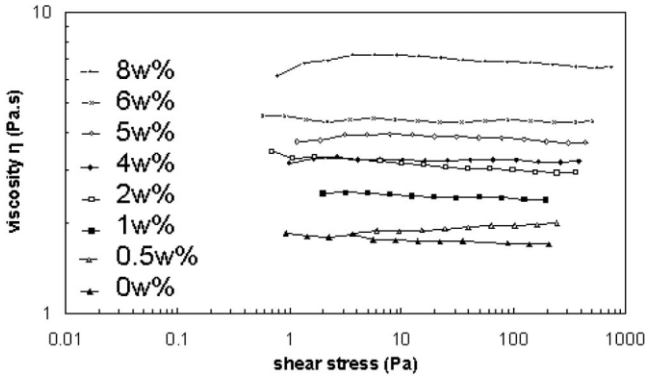

Figure 5 Viscosity/stress profile of acrylic PNC resins containing increasing C30B content.

At all concentrations of the silicate clay in the resin composition, we observe Newtonian flow. Increase of nanoparticle loading leads to an increase in viscosity. Since the viscosity of suspensions is considerably higher, when compared to that of the unfilled polymer matrix, one might imagine that the suspensions have become highly flocculated upon addition of the C30B particles to the acrylic polymer matrix. However, in that case the overall flow profile would become shear thinning by the shear-induced breakdown of flocculated structures which is not observed.

Another reason for the large increase in viscosity could be that the polymer–nanoparticle interactions are somewhat enhanced by hydrogen bonding between the acrylic polymer and the platelets edges, since the OH groups at the platelet edge are not completely blocked upon addition of the silane.

To examine the relaxation behavior of the nanocomposite resins, constant rate experiments were performed The torque from which the shear stress is determined is measured continuously, thus providing information on startup and steady state properties. To erase the sample history before performing the experiments, a shear rate of 800 s^{-1} was applied for 300 s.

Figure 6 shows the stress build up and relaxation at

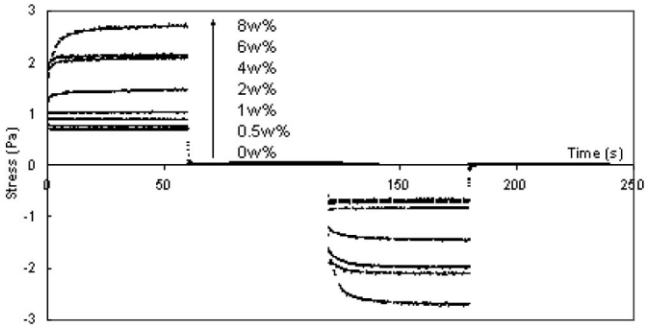

Figure 6 Relaxation curves PNC resins at 10% strain. PNC resins containing up to 8 wt % of Cloisite 30B were presheared at 800 s^{-1} before the measurements.

10% strain for suspensions containing 0 to 8 wt % of nanoparticles. The deformation rate was instantaneously applied, maintained constant for 60 s, and suddenly removed. After 60 s of 0 shear rate, the process is repeated in the opposite direction. The resulting stress curves comprise instantaneous, retarded and constant steady state stress followed by the same but with the reverse sign.

The constant-rate stress is due to viscous flow. The instantaneous stress and viscous flow were observed for all suspensions containing more than 2 wt % of filler loading and it increases linearly.

Morphological information from X-ray diffraction

In literature, X-ray powder diffraction in reflection or transmission is extensively used to characterize the structure of polymer nanocomposites (PNC). The extensive use of powder diffraction is largely based on the established procedures developed for the identification and structural characterization of layered silicate minerals.[5–7] The position, full width at half-maximum, and intensity of the (001) peak is used to characterize the morphology as immiscible, intercalated, or exfoliated. Nanocomposites are characterized by their large spacings (d001 $>$ 2.0 nm), which necessitates the collection of data at scattering angles of less than 10°. Layer disorder, silicate volume fractions less than 0.1, and experimental conditions all contribute to broadening and weakening of the peak, which introduces uncertainty in reliably determining layer–layer correlations. Vaia[8] stated that because of the strong dependence of experimental factors at low values of 2 è giving raise to artifacts, XRD should be complimented by microscopic observations, especially for PNC with low volume fractions of organically-modified layered silicates (OLS) that might have an exfoliated morphology. In practice, microscopy (i.e., transmission electron microscopy and atomic force microscopy) indicate that most systems fall short of the idealized morphology, more commonly exhibiting intermediate states or mixed structures.[7]

hkl Reflections in X-ray diffraction patterns

Of major interest for layered silicate-PNC is the relative distance and orientation of the inorganic layers, and not so much the crystal structure of the individual layers. The length scale of the former (1–4 nm) is approximately an order of magnitude larger than that of the latter (0.1–0.3 nm). Therefore, the scattering of interest for layered silicate-PNC characterization can be analyzed in terms of a random collection of crystallites consisting of 2D layers on a one-dimensional lattice. The *hk*0 reflections provide an internal standard for silicate concentration and, potentially, may provide information on the strain within the layers resulting from layer bending, deformation, or thermal history that the sample may have been exposed to.[9] The various clay mineral *hkl* reflections interfere with each other. A thick random powder specimen and a diffractogram with high peak to background resolution are needed. The peaks are weak, but can satisfactorily be resolved from the background by step scan procedures using long aquisition times. For crosslinked films using our set-up, this means a count time of 30 min to 2 h, while the amorphous resin nanocomposites need 5–10 h of count time. Unfortunately, the higher order reflections that we find as (110) at $2\theta_{\lambda\ 0.154\ \mathrm{nm}} = 23.15$, $q_{\lambda\ 0.154\ \mathrm{nm}} = 1.65$ are rarely discussed in the layered silicate-PNC literature.[5,6]

Analyzing polymer layered silicate nanocomposite scattering

C30B particle stacks have individual layers of ~0.98 nm thickness and a radius between 50 and 150 nm. Decreasing the mean stack size and increasing the fraction of individual layers broadens the basal reflections. Additionally, it lowers the magnitude of I ($q \rightarrow 0$), which is proportional to the mean size of the stacks.

Completely suspended clay scatters strongly at low q, where the scattering vector is $q = 4\pi\lambda^{-1} \sin(\theta)$.[10] Regardless of the layer composition in our samples, the structure factor increases markedly at low scattering angles. As required at low angles, the intensity increases with increasing clay content, whereas the lack of additional peaks confirms exfoliation.

The power-law dependence of I (q) at low q, smaller than the first basal reflection, approaches a slope -2 for highly dispersed thin plates. Scaling behavior in this regime for layered stacks is substantially less ($I \sim q^{m}$, $m < -2$). At high q (thickness of platelets ~1 nm), the use of the complete expression for the form factor of a (infinite) plate rather than the thin-plate approximation is required to correctly interpret the relative magnitudes of the reflections.[7] Experimentally, it is expected that polydispersity in lateral size, as well as lateral misalignment that yield an effective stack radius, which is larger than the radius of the individual platelets will smear the Guiner plateau that appears at q (radius of platelets) $<1\ \mathrm{nm}^{-1}$.

Atomic level details of the layer, not considered by the uniform plate description, produce additional features that should be considered for quantitative interpretation of higher order reflections at $q_{\mathrm{thickness}} > 1$ nm. The impact of the structure of the layer stacks (i.e., crystallites and tactoids) on the intensity for a large range of q emphasizes the importance of obtaining data with a high signal-to-noise ratio at both high ($q_{\mathrm{thicknes}} > 1$) and low ($q_{\mathrm{radius}} \sim 1$) q. For layered silicates, this will conservatively range from $0.05 < q < 2.1\ \mathrm{nm}^{-1}$ within the range of basal reflections of

intercalated systems.[11] The results shown in this article are for experimental reasons limited to the range of $0.15 < q < 1.8\ \text{nm}^{-1}$.

Morphology of the nanocomposites in the resin and cured state from X-ray diffraction

It is well known that a complete characterization of nanocomposites not only needs accurate analysis of the nanophase, it also requires information on the mesoscale and microscale (0.1–100 um). With all of these length scales being considered as factors, which may have been hidden before, orientational correlations and concentration fluctuations become apparent. Vaia[10] described the swelling of a layered silicate tactoid to an interlayer spacing greater than 10 nm, which does not imply a uniform distribution of inorganic layers on the micrometer scale. Even though XRD measurements may show that the interlayer spacing has increased to a single layer level, this is insufficient to prove an exfoliated morphology. It should also be kept in mind that systems are not necessarily monophasic. In practice, many systems appear to be mixtures of individual and stacked layers. This, combined with the high aspect ratio and grainy texture of the nanoparticles, gives rise to complex correlations within the systems, which cannot all be analyzed by means of XRD.

Figure 7(a) summarizes representative data sets for our acrylic nanocomposites resins with dispersed C30B, while Figure 7(b) comprises the data sets for cured acrylic nanocomposite films. The scattering curves are similar and show that no significant structural changes occur for concentrations from 0.5 to 8 wt % (equal to 0.0015 volume fraction to 0.0242 volume fraction). As the concentration of C30B increases, the scattered intensity increases for all q in the resin, as well as the cured film state. However at higher loadings, the presence of stack interaction peaks, for example, around $q = 4\ \text{nm}^{-1}$ to $q = 0.6\ \text{nm}^{-1}$ reveals the formation of stacks, indicating that the C30B particles are not fully exfoliated. The first characteristic distance inside the stacks can be estimated using $d_{[100]} = 2\pi/\text{q}$ leading to $d_{[100]} = 17.9$ nm for C30B intercalated acrylic resin and $d_{[100]} = 15.7$ nm for crosslinked C30B intercalated resin. In contrast to the crosslinked films at all silicate concentrations, the resin samples exhibit broader, less intense (001) reflections. This is considered representative of a more disordered system. Beside the intensity difference between disordered systems [noncrosslinked, Fig. 7(a)] and to some extent ordered systems [crosslinked films, Fig. 7(b)], it is plausible to consider that crosslinking of the material at high temperatures gives rise to a certain amount of restacking of the layers, since they are driven together by depletion interactions with the growing polymer chains.

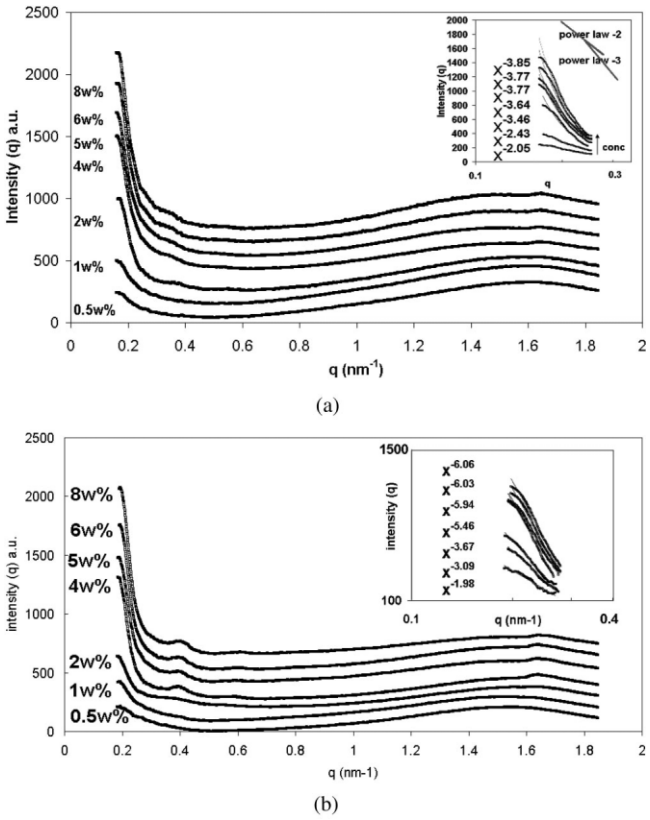

Figure 7 X-ray diffraction patterns of PNC's containing increasing Cloisite 30B content. (a) Patterns of nanocomposite resins; and (b) patterns of nanocomposite films.

These somewhat qualitative results obtained from Figure 7 are insufficient to establish complete structure–property relationships. Quantifiable data such as particle–particle distance, relative orientation of particles, fraction of individual layers, and particle number density are preferred.

Analysis of the modulus of cured nanocomposite resins

The aspect ratio of the reinforcing particles in each nanocomposite is calculated using the Halpin–Tsai model, by comparing the measured modulus of the nanocomposites with that of the unfilled matrix. The modulus of coating films is strongly influenced by the amount of crosslinking, therefore extra care has been taken to assure that the sample films were completely cured to avoid a change in the modulus of the matrix material without actually changing the microstructure of the nanocomposite.

The Halpin–Tsai model[12,13] can be used to provide a relatively simple model for determining the aspect ratio of the reinforcing particles. Polydispersity of the reinforcing particles leads to an average particle aspect ratio.

The Halpin–Tsai equation is shown in eq. (2)

$$E_c = E_m \frac{E_f(1 + \zeta\phi_f) + E_m(\zeta - \zeta\phi_f)}{E_f(1 - \phi_f) + E_m(\zeta + \phi_f)} \quad (2)$$

where E_c is the composite Young's modulus, E_f the filler modulus, E_m the matrix modulus, ζ the shape factor, which depends on the geometry, orientation and aspect ratio of the particles, and φ_f the volume fraction filler. The shape factors for the tensile moduli of platelet reinforced composites are[9] E_{11} or E_{22} $\zeta = 2/3 \cdot (w/t)$ (in the radial direction of the platelets), E_{33} $\zeta = 2$ (perpendicular to the platelets), and (w/t) = width of platelet/thickness of platelet = aspect ratio.

When the aspect ratios are much smaller than the ratio of filler and matrix modulus ($\zeta << E_f/E_m$), the Halpin–Tsai model gives results close to a series model, while if the aspect ratios are much larger than the ratio of filler and matrix modulus ($\zeta >> E_f/E_m$), the Halpin–Tsai model gives results close to a parallel model. For nanocomposites, the series model underestimates the modulus, because the volume fraction of filler is very low, and thus yields values close to the matrix modulus. However, the parallel model overestimates the composite modulus at low matrix moduli, since it assumes a continuous reinforcing phase. The Halpin–Tsai model [eq. (2)] leads to results that are in between these two extremes, when the aspect ratio is of the same order of magnitude as the ratio of moduli ($\zeta \approx E_f/E_m$). The aspect ratio of the particles has a strong influence on the results and, therefore, determines how close the results are to either the series or parallel model. The influence of the aspect ratio and, therefore, also of the level of exfoliation on the modulus is very important. Platelets aspect ratios for layered silicate nanocomposites are typically around 100–200; consequently when exfoliation is not optimal, the resulting reduction in the effective aspect ratio has a large effect on the modulus. The Halpin–Tsai model can be used to calculate the aspect ratio of the reinforcing particles when the modulus of the composite, matrix, and filler are known. The Halpin–Tsai model only gives an *effective* aspect ratio, because the particles can have different shapes, sizes, and thicknesses. The effective aspect ratio represents the best fit with the measured moduli and can be considered a useful parameter to compare different nanocomposite compositions, as well as providing a reasonable estimate of the achieved level of exfoliation.

The reinforcement that causes increase in modulus when nanofillers are added to polymers are often assumed, in the literature, to be because of the reduced mobility of a constrained polymer phase close to the silicate layers. The large surface area of the exfoliated platelets is assumed to be responsible for this constrained polymer phase with a higher modulus.[14–16] The increased reinforcement of the whole composite benefits from strong ionic bonds between the polymer and the silicate platelets, using more traditional composite models.[17] The modulus of the composite is expected to be influenced by the modulus of the matrix, the modulus of the filler, and the shape and orientation of the filler particles.[18,19]

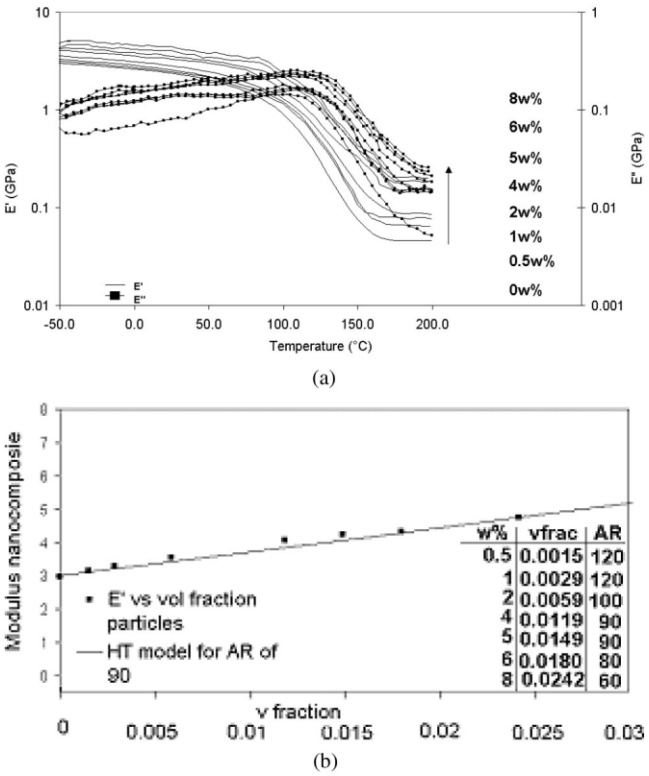

Figure 8 (a) DTMA results in the cured film of C30B-carylate resin. (b) The expected moduli according to the HS model for a aspect ratio of 120.

The measured results for the tensile modulus of the nanocomposite samples at various silicate concentrations are shown in Figure 8(a), along with the calculated aspect ratios (AR) from the HT model as shown in Figure 8(b).

Over the whole range, an increase in Youngs modulus is clear. The effect is most pronounced above T_g, with the largest increase occurring at higher silicate loadings (Table II).

The measured matrix modulus of the unfilled system is used in the Halpin–Tsai model to calculate the effective aspect ratio. The calculated effective aspect ratios are determined assuming that the particles are aligned with their long axes along the test axis, which is a reasonable assumption according to the TEM results shown in the next section. It can be seen from Figure 8(b) that the effective aspect ratio decreases with increasing silicate content, which can be explained by a less effective exfoliation at higher silicate loadings. The reduced exfoliation at higher silicate content has been reported previously by several authors.[20–22] With increasing concentration, the exfoliation becomes less perfect, resulting in an effective

TABLE II
Increase in Moduli Above and Below T_g of the Cured PNC Resins According to the DTMA Results

		Below T_g at 24.7°C				Above T_g at 154.6°C			
w% C30B	vfr C30B	E'	Incr E' (%)	E''	Incr E' (%)	E'	Incr E' (%)	E'	Incr E'' (%)
0	0	2.38405		0.08044		0.0632		0.02218	
0.5	0.0015	2.46826	103	0.13631	169	0.0920	144	0.03559	160
1	0.0029	2.57829	108	0.14299	177	0.8901	140	0.03734	168
2	0.0059	2.83809	19	0.14044	174	0.1409	221	0.04824	217
4	0.0119	3.32719	139	0.16675	207	0.2466	388	0.05573	251
5	0.0149	3.54071	148	0.17502	217	0.3056	481	0.06920	311
6	0.0180	4.03955	169	0.15944	198	0.6058	953	0.14905	672
8	0.0242	4.59760	193	0.17399	216	1.0198	1605	0.22107	996

aspect ratio that is approximately half of the highest value at low filler concentration. It has to be mentioned that especially at low silicate contents, the calculation of the effective aspect ratio is rather sensitive to the error in the modulus measurements.

TEM analysis of cured films

TEM analysis of the four cured nanocomposite resins was performed. Figure 9(a–d) shows an overview of the obtained TEM results.

At a silicate concentration of 1 wt %, mostly individual silicate platelets can be observed with a significant amount of them oriented in the longitudinal direction. At higher silicate loadings of 2 and 5 wt %, an increase in stacking is observed, where almost all the silicate layers are oriented in the longitudinal direction. In the stacks, a layer distance of ~15 nm can be found in good agreement with the XRD measurements discussed in the Morphology of the Nanocomposites in the Resin and Cured State from X-ray Diffraction section.

At the highest silicate loading of 8 wt %, the first picture shows a dispersion of agglomerated platelets. This sample consists of well-dispersed agglomerates together with individual platelets, where the layer distance within the stacks is ~5 nm. As TEM analysis is a very visual tool, care has to be taken with the interpretation of the results. Errors are likely to occur if the conclusions on the morphology the samples are based on the examination of a few local regions within a sample. Especially using high aspect ratio particles, such as layered silicates, the sample preparation and processing history will not only result in preferential particle alignment but also in a skin-core structure with different particle concentration and alignment occurring near the surface and in the bulk of the sample.

CONCLUSIONS

A route for the preparation of C30B filled acrylic-based nanocomposite resins is described. This route yields nanocomposite resins in organic solvent, which in a second stage can be emulsified to form nanocomposite resin emulsions where the nanoparticles are located inside the emulsion droplets. Various experimental techniques were used to characterize the nanoparticle resin dispersions and cured films, namely rheology, X-ray diffraction, DMTA, TEM, also keeping in mind the shear rates involved in the envisaged coating process.

For the dispersion route described in this manuscript, it is shown that up to 2 wt % of silicate loading mainly exfoliated platelets are present. At higher silicate loading, stacking is observed with a *d*-spacing of ~15 nm. DMTA measurements show that there is a significant improvement of modulus upon addition of high aspect ratio silicate platelets, especially above T_g of the cured resin. The rate of increase in the modulus of the cured free standing films is reduced at higher silicate loading. This is consistent with the outcome of effective aspect ratio determination based on the Halpin–Tsai theory. At the highest concentration of 8 wt % silicate, the effective aspect ratio is only half of that determined at the lowest concentration. It is shown that at higher silicate loading, the solid-like rheology of the material starts to dominate, making the samples resistant to flow. This is a major disadvantage for processing of the resins and also gives rise to poor leveling during the curing process.

TEM analysis at all loadings shows a homogeneous dispersion of particles (which are in the form of separate platelets at low silicate loadings and aggregated stacks at higher silicate loadings) in the polymer matrix. Cross-sectional images of the cured films at all concentrations indicate spontaneous alignment of the high aspect ratio plate-like C30B particles in the plane of the film

As a final remark it should be mentioned that strengthening of the polymer–nanoparticle interface is critical to manage stress transfer during deformation of the final cured film. A methodology to increase this would involve the use of *in situ* compatibilization, whereby either the nanoplatelets or the matrix poly-

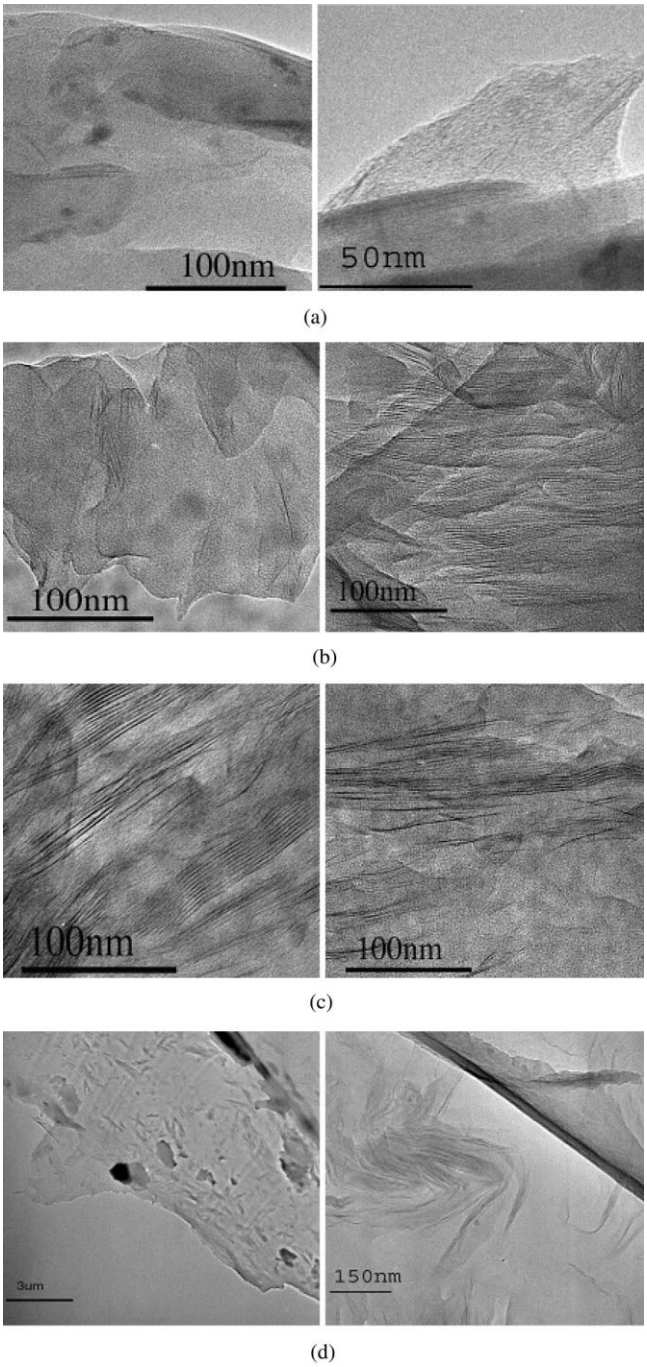

Figure 9 TEM micrographs of acrylic PNC's containing (a) 1 wt %, (b) 2 wt %, (c) 5 wt % and (d) 8 wt % Cloisite 30B.

mer would be chemically designed so as to actually react with the other and form covalent bonds with it during the crosslinking process.

Akzo Nobel Chemicals and Nuplex Resins (previously Akzo Nobel Resins) are kindly acknowledged for providing the resins and for guidance. We acknowledge in particular Dr. M. Bosma and M. van der Horst (AN-Chemicals) for the DTMA measurements and Dr. C. Vijverberg, Dr. F. van Wijk and Dr. A. Roelofs(Nuplex resins) for all their support. Dr. P.J. Kooyman of the National Center for High Resolution Electron Microscopy, TU Delft is acknowledged for the TEM analysis. B. Norder and G. de Vos of Polymer and Materials Engineering, and TU Delft are acknowledged for the rheological measurements and TEM sample preparation.

References

1. Sam Brauer. P-234R Polymer nanocomposites: Nanoparticles, nanoclays and nanotubes; Business Communications Company, April 2004.
2. EET Internal Reports ; Innovative water borne automotive resins 2002–2005.
3. Nienhaus et al. U.S. Pat. No. 5,670,600 (1997). Assignee: BASF.
4. Bosma, M. Akzo Nobel Chemicals, personal communication.
5. Bish, D. L.; Post, J. E., Eds. Modern Powder Diffraction: Reviews in Mineralogy, Vol. 20; Mineralogical Society of America: Washington, DC, 1989.
6. Brindely, G. W.; Brown, G. Clay Minerals and Their X-Ray Identification; Crystal Structure of Society: London, 1980.
7. Moore, D. M.; Reynolds, R. C. X-Ray Diffraction and the Identification and Analysis of Clay Minerals; Oxford University Press: New York, 1997.
8. Vaia, R. A. In Polymer Clay Nanocomposites; Pinniavaia, T. J.; Beall, G. W., Eds.; Wiley: New York, 2000.
9. Vaia, R. A.; Liu, W. J Polym Sci Part B: Polym Phys, 2002, 40, 1590.
10. Roe, R. J. Methods of X-Ray and Neutron Scattering Polymer Science; Oxford University Press: New York, 2000; p 155.
11. Krishnamoorti, R.; Vaia, R. A., Eds.; ACS Symposium; American Chem Society: Washington, DC, 2001; p 99.
12. Halpin, J. C.; Kardos, J. L. Polym Eng Sci 1976, 16, 344.
13. Halpin, J. C. J Compos Mater 1969, 3, 732.
14. Yoon, P. J.; Fornes, T. D.; Paul, D. R. Polymer 2002, 43, 6727.
15. Shelley, J. S.; Mather, P. T.; DeVries, K. L. Polymer 2001, 42, 5849.
16. Giannelis, E. P. Adv Mater 1996, 8, 29.
17. Usuki, A.; Koiwai, A.; Kojima, Y.; Kawasumi, M.; Okada, A.; Kurauchi, T.; Kamigaito, O. J Appl Polym Sci 1995, 55, 119.
18. Es, M. A. v.; Xiqiao, F.; Turnhout, J. v.; Giessen, E. v. d. Specialty Polymer Additives, Blackwell Science: London, 2001; Chapter 21.
19. Fornes, T. D.; Paul, D. R. Polymer 2003, 44, 4993.
20. Akkapeddi, M. K. Polym Compos 2000, 21, 576.
21. Es, M. A. v. Ph D. Thesis, Delft University of Technology, 2001.
22. Liu, L.; Qi, Z.; Zhu, X. J Appl Polym Sci 1999, 71, 1133.